CHEMISTRY
A European Journal

www.chemeurj.org

Reprint

A Journal of
ChemPubSoc Europe
ACES
Asian Chemical Editorial Society
WILEY-VCH

ChemPubSoc Europe

DOI: 10.1002/chem.201800060

CHEMISTRY A European Journal Full Paper

Macrocyclic Photosensitizer

Proton-Dependent Switching of a Novel Amino Chlorin Derivative as a Fluorescent Probe and Photosensitizer for Acidic Media

Daniel A. Heredia,[a] Andrés M. Durantini,[a] Ariel M. Sarotti,[b] Natalia S. Gsponer,[a] Darío D. Ferreyra,[a] Sonia G. Bertolotti,[a] María E. Milanesio,[a] and Edgardo N. Durantini*[a]

Abstract: A novel chlorin derivative ($TPCF_{20}$-NMe_2) has been synthesized as a *syn* adduct of a pyrrolidine-fused chlorin bearing a C-linked *N*,*N*-dimethylaminophenyl residue. The absorption spectrum of $TPCF_{20}$-NMe_2 is essentially identical to that of $TPCF_{20}$ in *N*,*N*-dimethylformamide, indicating a very weak interaction between the chlorin macrocycle and the amine group in the ground state. However, the fluorescence emission of the chlorin moiety in $TPCF_{20}$-NMe_2 is effectively quenched by the attached amine unit. Moreover, $TPCF_{20}$-NMe_2 is unable to attain a triplet excited state or to photosensitize singlet molecular oxygen. Spectroscopic and redox properties indicate that intramolecular photoinduced electron transfer can take place from the *N*,*N*-dimethylaminophenyl group to the chlorin macrocycle. Thus, in an acid medium, protonation of the amino group leads to a considerable increase in the fluorescence emission, triplet excited-state formation, and singlet molecular oxygen production. Photodynamic inactivation of *Escherichia coli* sensitized by $TPCF_{20}$-NMe_2 is negligible at neutral pH. However, this chlorin becomes highly effective in inactivating *E. coli* cells under acidic conditions. Therefore, these results indicate that $TPCF_{20}$-NMe_2 is an interesting molecular structure, in which protonation of the amino group can be used as an off/on molecular switch activating red fluorescence emission and photodynamic activity capable of eradicating bacteria.

Introduction

Chlorin macrocycles are essential for the development of life on this planet.[1] Photosynthesis would not be possible without the light-harvesting and trapping activities of reduced porphyrins. In addition to the biosynthetic process, most chlorins can be synthesized from porphyrins with different substitution patterns at the periphery of the tetrapyrrolic macrocycle.[2] In particular, symmetrically *meso*-substituted porphyrins can be easily obtained in one-pot syntheses from an aldehyde and pyrrole according to a modification of Lindsey's method.[3] In these compounds, reduction of one pyrrole ring yields the chlorin chromophore bearing an annulated five-membered ring. Moreover, porphyrins can be used to obtain chlorins with amphiphilic structural features by cycloaddition of diverse entities at the β,β′-positions of the macrocycle.[2] In this regard, 1,3-dipolar cycloaddition reactions are an effective approach for the synthesis of five-membered heterocycles. Electron-deficient carbonyl ylides are known to react with many dipolarophiles. In 1,3-dipolar cycloadditions, the peripheral pyrrolic double bonds of porphyrins (dipolarophiles) react with azomethine ylides (1,3-dipoles), which are prepared in situ from an aldehyde and an α-amino acid. Thermal decarboxylation of the resulting imine gives the corresponding 1,3-dipole. Thus, *meso*-tetraarylporphyrins have been used as dipolarophiles with azomethine ylides to produce chlorins and isobacteriochlorins.[4] It has been demonstrated that the presence of electron-withdrawing atoms in the aryl substituents increases the reactivity of the porphyrins towards azomethine ylides. Moreover, calculations of reaction pathways have been performed to demonstrate that cycloadditions of azomethine ylides to porphyrins are irreversible and kinetically controlled.[5]

Chlorin derivatives, distinct from porphyrins, show an intense absorption band at around 650 nm.[1] This is an important feature in biomedical applications as absorption in the phototherapeutic window produces a deeper penetration of light into tissue.[6] Therefore, chlorins constitute interesting theranostic agents because their intense red fluorescence emission allows diagnostic imaging, and the long lifetimes of their triplet excited states can be exploited to efficiently produce reactive oxygen species (ROS) in photodynamic therapy.[7,8] In addition, chlorins have also been proposed as photosensitizers with potential applications in photodynamic inactivation (PDI) of microorganisms.[9] This approach is based on the accumulation of a photosensitizer in microbial cells.[10] Irra-

[a] Dr. D. A. Heredia, Dr. A. M. Durantini, Dr. N. S. Gsponer, Dr. D. D. Ferreyra, Prof. S. G. Bertolotti, Dr. M. E. Milanesio, Prof. E. N. Durantini
Departamento de Química, Facultad de Ciencias Exactas
Físico-Químicas y Naturales, Universidad Nacional de Río Cuarto
Ruta Nacional 36 Km 601, X5804BYA Río Cuarto, Córdoba (Argentina)
Fax:(+54) 358-4676233
E-mail: edurantini@exa.unrc.edu.ar

[b] Prof. A. M. Sarotti
Instituto de Química Rosario (CONICET)
Facultad de Ciencias Bioquímicas y Farmacéuticas
Universidad Nacional de Rosario
Suipacha 531, 2000 Rosario, Santa Fe (Argentina)

Supporting information and the ORCID number(s) for the author(s) of this article can be found under https://doi.org/10.1002/chem.201800060.

diation with visible light excites the photosensitizer, which induces the formation of ROS under aerobiosis. These reactive species react with the surrounding biomolecules in the cell, leading to a loss of biological functionality and consequent cell death.[11] The development of this alternative therapy for the treatment of microbial infections is being driven by the global appearance of multidrug-resistant bacteria, which pose an increasing risk to antibiotic therapy.[12] In particular, *Escherichia coli* bacteria can cause severe hospital-acquired infections.[13] These Gram-negative bacteria present high-level resistance to most classes of antibiotics due to the expulsion of antimicrobial drugs by multidrug efflux pumps and the impermeability of the bacterial outer membrane.[14] In this context, chlorin derivatives have been regarded as promising for the treatment of bacterial infections under red light.[15–18] These compounds contain intrinsic cationic centers or bear aliphatic amine substituents as precursors of positive charges at physiological pH. Moreover, *E. coli* is capable of surviving under extreme acid pH stress for several hours.[19] The human digestive tract represents a major host barrier against exogenous microorganisms. However, the acid resistance of *E. coli* to gastric fluid may be implicated in several diseases.[20,21] There is variability in the pH of human gastric fluid, but little information is available concerning PDI of *E. coli* in extremely acidic media.

In this work, a novel chlorin derivative ($TPCF_{20}$-NMe_2, Scheme 1) was synthesized by 1,3-dipolar cycloaddition reaction using 5,10,15,20-tetrakis(pentafluorophenyl)porphyrin ($TPPF_{20}$) as a dipolarophile, and *N*,*N*-dimethylaminobenzaldehyde and *N*-methylglycine to form the azomethine ylide. $TPCF_{20}$-NMe_2 contains a pyrrolidine-fused ring bearing a C-linked *N*,*N*-dimethylaminophenyl residue. The new compound is based on a two-segment structure, consisting of a chlorin macrocycle substituted by pentafluorophenyl electron-withdrawing groups and an electron-donor amine group. Therefore, we report for the first time a chlorin-based molecular switch, in which photoinduced electron transfer (PeT) from the amine segment to the chlorin macrocycle effectively competes with fluorescence emission and intersystem crossing, thereby reducing formation of the triplet state. The solution spectroscopic properties and photodynamic activities of $TPCF_{20}$-NMe_2 have been compared in vitro using a Gram-negative bacterial species *Escherichia coli* with the addition of acid media. This investigation demonstrates that a photosensitizer derived from chlorin can be effective in identifying and eradicating *E. coli* under extreme acid conditions, while remaining inactive at neutral pH.

Results and Discussion

Synthesis of chlorins

A novel chlorin derivative was synthesized by a 1,3-dipolar cycloaddition reaction between $TPPF_{20}$ and an azomethine ylide, generated from 4-(*N*,*N*-dimethylamino)benzaldehyde and *N*-methylglycine in dry toluene (Scheme 1). The strongly electron-withdrawing substituents in the *meso* positions of $TPPF_{20}$ induce an electron-deficient π system in the peripheral double bonds of the macrocycle. This effect increases the dipolarophile character of the porphyrin.[4,22,23] The presence of an electron-donating group on the aldehyde reinforces the 1,3-dipole, since it imparts stability to the azomethine ylide by delocalization of the positive charge.[4] The solution was stirred under reflux for 18 h in an argon atmosphere. The reaction was monitored by UV/Vis absorbance spectroscopy, following the growth of the characteristic chlorin band at 650 nm (Figure S1).[17] The formation of isobacteriochlorins or bacteriochlorins by a second cycloaddition to another double bond, which would have given bands at around 588 and 750 nm, respectively,[17,18] was not detected. However, TLC analysis (silica gel; toluene/ethyl acetate, 9:1) revealed the formation of two adducts. The respective spots appeared green under visible light, characteristic of chlorins, although under UV light only one of them appeared fluorescent. After isolation of each individual product by chromatography (silica gel), their UV/Vis spectra suggested that chlorins had been formed.

The first-eluted green band showed red fluorescence emission and was identified as the unexpected chlorin $TPCF_{20}$ in 28% yield. The formation of $TPCF_{20}$ was unambiguously confirmed by examination of its ^{1}H NMR spectrum and comparison with previously published literature data.[17] The synthesis of $TCPF_{20}$ is generally performed under similar conditions, but using formaldehyde.[4] However, formaldehyde can be formed by Strecker degradation of *N*-methylglycine, as shown in Scheme 2.[24] Hence, $TPCF_{20}$ could also be obtained by reaction of $TPPF_{20}$ with *N*-methylglycine in refluxing toluene. This experiment has been performed previously and afforded $TCPF_{20}$ in 36% yield after heating the mixture under reflux in toluene for three days.[25]

The second-eluted green band did not show emission after exposure to UV light. HR-MS experiments indicated the appending of a 4-(dimethylamino)benzaldehyde moiety by the 1,3-dipolar cycloaddition to $TPPF_{20}$. At first, we supposed the formation of two diastereoisomers of $TPCF_{20}$-NMe_2 as a conse-

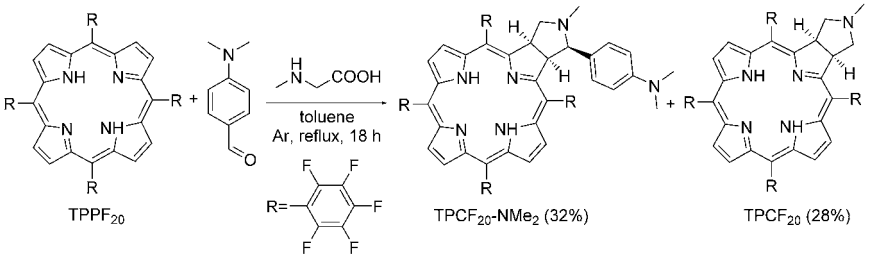

Scheme 1. Synthesis of chlorins $TPCF_{20}$-NMe_2 and $TPCF_{20}$.

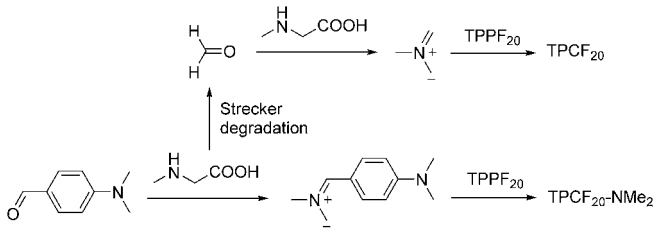

Scheme 2. 1,3-Dipolar cycloaddition pathways involved in the formation of $TPCF_{20}$-NMe_2 and $TPCF_{20}$.

quence of *endo* and *exo* cycloadditions, leading to the *anti* and *syn* adducts (Figure 1). However, after a series of chromatographic purifications, only one possible adduct was isolated in 32% yield. To determine the structure of this adduct, theoretical calculations and NMR studies were carried out.

Signal assignments in the ^{1}H NMR spectrum of $TPCF_{20}$-NMe_2 are listed in Table 1. In the aromatic region, as a consequence of the asymmetric functionalization of the macrocycle, four of the six β-pyrrolic protons give rise to four doublets with different coupling constants, at $\delta = 8.12$ and 8.51 ppm ($J = 5.0$ Hz) and at $\delta = 8.41$ and 8.69 ppm ($J = 4.7$ Hz). The remaining two β-pyrrolic protons give rise to an AB system at $\delta = 8.45$ ppm. The aromatic protons of the *N*,*N*-dimethylaniline moiety give rise to doublets at $\delta = 5.65$ and 5.85 ppm ($J = 8.8$ Hz). These anomalous chemical shifts can be rationalized by taking into account that this moiety is located over the tetrapyrrolic ring, where it is subject to a ring-current effect. In the aliphatic region, a singlet at $\delta = 2.56$ ppm can be assigned to the six -$N(CH_3)_2$ protons. Furthermore, the methylene protons on the pyrrolidinic ring give rise to signals at $\delta = 2.87$ and 3.56 ppm, with a geminal coupling constant of 9.7 Hz. The methine proton resonance was assigned as a doublet at $\delta = 3.63$ ppm. Additionally, the spectrum features two signals at $\delta = 5.36$ and 5.68 ppm attributable to the two β-pyrrolic protons of the reduced ring H_3 and H_2, respectively. Coupling constant analysis indicated that H_3 and H_{4b} have $J = 0$ Hz, indicating a *trans* configuration (dihedral angle approximately 90°). This confirmed that the cycloaddition proceeded in an *endo* fashion. Finally, in the downfield region, a singlet corresponding to the methyl group is observed at $\delta = 1.75$ ppm. More details concerning the *syn* and *anti* cycloadducts were determined through computational calculations.

Table 1. Experimental and calculated chemical shifts of *syn* and *anti* isomers in chloroform.

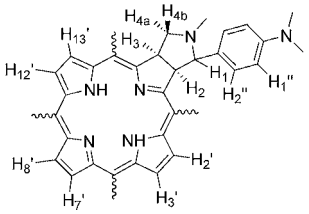

Proton	δ_{exp}	δ_{calc} (*anti*)	δ_{calc} (*syn*)
H_1	3.63	3.16	3.44
H_2	5.68	5.61	5.51
H_3	5.36	5.70	5.39
H_{4a}	2.87	2.77	2.90
H_{4b}	3.56	3.76	3.87
NMe	1.75	1.85	1.63
H-1′′	5.85	6.41	5.65
H-2′′	5.65	6.39	5.47
Ar-NMe_2	2.56	3.08	2.66
H-2′	8.12	8.43	8.06
H-3′	8.51	8.61	8.54
H-7′	8.45	8.54	8.56
H-8′	8.45	8.31	8.69
H-12′	8.69	8.76	8.59
H-13′	8.41	8.28	8.53

For this purpose, the global minimum geometries were initially determined after exhaustive exploration of the potential energy surfaces (PES) of the two candidate structures (including the tautomerism at the chlorin system) at the B3LYP/6-31 G* level of theory. As shown in Figure 1, an important stereochemical consequence of the *syn* adduct is that the *N*,*N*-dimethylaminophenyl group lies above the macrocycle, and consequently the aromatic protons should be more affected by the anisotropy exerted by the chlorin system. This observation is in good agreement with the significant shielding observed for these protons in the ^{1}H NMR spectrum of $TPCF_{20}$-NMe_2 ($\delta =$ 5.65 and 5.85 ppm). In order to provide further insight, we next computed the NMR shifts at the PCM/mPW1PW91/6–31 + G** level of theory (using chloroform as solvent), which in turn were used to assign the signals in the experimental spectrum. As is evident from Table 1, much better agreement between experimental and calculated data was observed for the *syn* isomer, with MAE (mean average error) and MaxErr (maximum

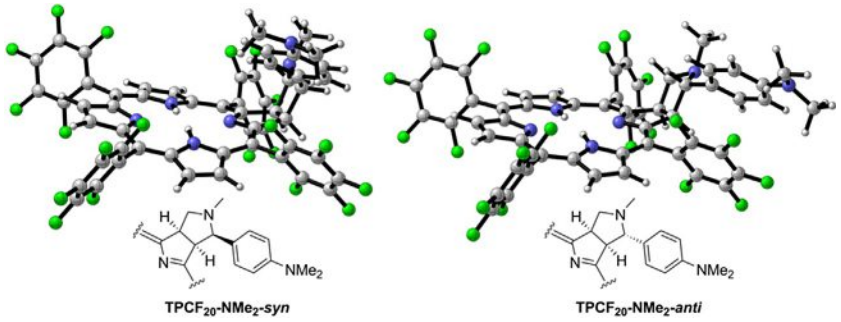

Figure 1. B3LYP/6-31 G* global minimum structures located for the *syn* and *anti* adducts of $TPCF_{20}$-NMe_2.

error) values of 0.13 ppm and 0.30 ppm, respectively, lower than those computed for the *anti* adduct (0.26 ppm and 0.74 ppm, respectively). Interestingly, our calculations correctly reproduced the significant shielding of the aromatic protons in the *syn* isomer ($\delta_{exp}=5.65$ and 5.85 ppm; $\delta_{calc}=5.47$ and 5.65 ppm). We also estimated the coupling constants (*J*) using the well-known Karplus–Conroy equation from the dihedral angles (ϕ) computed from the B3LYP/6-31 G* global minimum geometries found for each isomer. As shown in Table 2, predictions made for the *syn* adduct showed a better match with the experimental values than those for the *anti* adduct, mainly in the coupling between H-3 and H-4b. Finally, we carried out DP4+ calculations to reinforce our assignment; as expected, the results were conclusively in favor of the *syn* isomer with high confidence (>99.9%).

Table 2. Experimental and calculated neighborhood coupling constants (*J*) and calculated dihedral angles (ϕ).

Angles	ϕ (*syn*) [°]	ϕ (*anti*) [°]	J_{exp} [Hz]	J_{cal} (*syn*) [Hz]	J_{cal} (*anti*) [Hz]
H_1/H_2	24.9	157.3	8.8	7.9	12.5
H_3/H_{4a}	32.0	13.3	7.3	6.9	9.2
H_3/H_{4b}	89.0	133.5	0.0	0.3	6.8

Absorption and fluorescence spectroscopic characterization

Absorption spectra of the porphyrin $TPPF_{20}$ and the chlorins $TPCF_{20}$ and $TPCF_{20}$-NMe_2 were first compared in DMF, as shown in Figure 2. The main optical characteristics are summarized in Table 3. All of the spectra feature an intense Soret absorption band in the region 400–420 nm, with a molar absorption coefficient of the order of $10^5\,M^{-1}cm^{-1}$. The sharp Soret band absorptions indicate that the photosensitizers are dissolved as monomers in DMF.[18] All of the macrocycles present four Q-bands in the visible region between 500 and 700 nm. $TPPF_{20}$ has a typical spectrum of the *phyllo* type, with relative intensities of $\varepsilon_{IV}>\varepsilon_{II}>\varepsilon_{III}>\varepsilon_{I}$, whereas for the chlorins $TPCF_{20}$ and $TPCF_{20}$-NMe_2 the order is $\varepsilon_{I}>\varepsilon_{IV}\approx\varepsilon_{III}>\varepsilon_{II}$. Chlorin derivatives show a higher Q_x(0-0) band absorbance as a consequence of reduction of the porphyrin ring. This effect produces an intense absorption of chlorins at around 650 nm, distinct from that of porphyrins.[26]

Table 3. Spectroscopic characteristics of chlorin derivatives in DMF.

Chlorin	λ_{max}^{Soret}	$\varepsilon^{Soret[a]}$	λ_{max}^{Ql}	$\varepsilon^{Ql[a]}$	λ_{max}^{em}	E_s [eV][b]	Φ_F[c]
$TPCF_{20}$	404	1.98×10^5	650	5.31×10^4	653	1.90	0.16 ± 0.02
$TPCF_{20}$-NMe_2	405	1.79×10^5	651	4.71×10^4	653	1.90	$(1.9\pm0.2)\times10^{-3}$

[a] Molar absorption coefficient ($L\,mol^{-1}\,cm^{-1}$); [b] energy levels of the singlet excited states; [c] fluorescence quantum yields.

For comparison, time-dependent density functional theory (TDDFT) calculations were carried out at the CAM-B3LYP/6-31 G* level of theory on the first ten vertical excitations of $TPCF_{20}$-NMe_2. As shown in Table S1, the Q_x band is predicted at 590 nm (ca. 60 nm lower than experimentally observed, a characteristic offset for related systems at similar levels of theory),[27–29] and is mainly composed of the HOMO→LUMO (74%) and a smaller proportion of the HOMO−2→LUMO+1 (23%). The second transition (500 nm) corresponds to the Q_y band, with HOMO−2→LUMO (58%) and HOMO→LUMO+1 (38%) as the main transitions, with a minor component of HOMO−1→LUMO (3%). A third transition was computed at 399 nm, mainly composed of the HOMO−1→LUMO excitation (94%), which can be assigned as a charge-transfer excitation. The following two transitions at 360 and 354 nm, with high oscillator strengths (1.5059 and 1.0799, respectively) mainly correspond to HOMO→LUMO+1 (61%) and HOMO−2→LUMO+1 (65%), respectively, characteristic of the B_x and B_y bands. Figure S2 shows the key frontier molecular orbitals (FMOs) corresponding to these transitions, computed at the CAM-B3LYP/6-31 G* level of theory.

The fluorescence emission spectra of these chlorins and $TPPF_{20}$ were recorded in DMF. As shown in Figure 3, the spectrum of $TPCF_{20}$ features two emission bands in the red region at around 650 and 710 nm, attributable to the Q(0-0) and Q(0-1) transitions.[18,26] These red emissions are characteristic of chlorin derivatives. The Q(0-0) and Q(0-1) transitions correspond to decays from the first singlet excited state to the first

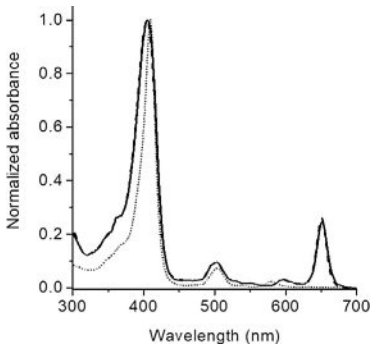

Figure 2. Normalized absorption spectra of $TPCF_{20}$-NMe_2 (solid line), $TPCF_{20}$ (dashed line), and $TPPF_{20}$ (dotted line) in DMF.

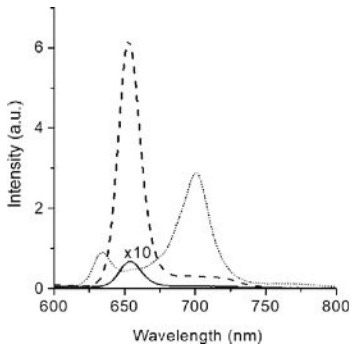

Figure 3. Fluorescence emission spectra of $TPCF_{20}$-NMe_2 (×10, solid line), $TPCF_{20}$ (dashed line), and $TPPF_{20}$ (dotted line) in DMF ($\lambda_{exc}=507$ nm).

two vibrational levels of the ground state (0 and 1, respectively). $TPCF_{20}$-NMe_2 also showed two red emission bands and it appeared slightly fluorescent in comparison with $TPCF_{20}$. Stokes shifts were calculated from the intersection of the absorption and fluorescence spectra of the Q_x(0-0) band. Small Stokes shifts of 2 and 3 nm were determined for $TPCF_{20}$ and $TPCF_{20}$-NMe_2, respectively. These small Stokes shift indicated that the spectroscopic energies of the chlorins were similar to the relaxed energies of their singlet states. Thus, only minor structural changes occur between their ground and excited states, reflecting the rigid planar structure of the tetrapyrrolic macrocycle. Taking into account the energies of the 0-0 electronic transitions, the energy levels of the singlet excited stated (E_s) were estimated (Table 3) from the intersection of the normalized absorption and fluorescence spectra. As expected, the E_s values are very similar to those previously reported for chlorin derivatives.[18] Moreover, the normalized fluorescence excitation spectra of $TPCF_{20}$ and $TPCF_{20}$-NMe_2 in DMF were compared (Figure S3). The excitation spectra of these chlorins were found to be similar to the absorption spectra (Figure 2). Therefore, $TPCF_{20}$ and $TPCF_{20}$-NMe_2 were mainly dissolved as monomers in this organic solvent.

The fluorescence quantum yields (Φ_F) of these macrocycles in DMF were calculated by comparison with that of the reference 5,10,15,20-tetrakis(4-methoxyphenyl)porphyrin (TMPP). The results are summarized in Table 3. The value of Φ_F for $TPCF_{20}$ matched that reported previously.[17] Similar values are expected for *meso*-phenyl-substituted chlorin derivatives.[18,30] However, a very low Φ_F (Table 3) was determined for $TPCF_{20}$-NMe_2, which is an unusual value for chlorins. As can be observed in Figure S4 A, $TPCF_{20}$-NMe_2 does not exhibit a red fluorescence emission akin to that from a solution of $TPCF_{20}$, despite both having the same absorbance at the Soret band and being irradiated with UV light. This result indicates strong quenching of the excited singlet state of the chlorin by the attached *N*,*N*-dimethylaminophenyl moiety. The quenching efficiency of the macrocycle emission was $\eta_q \geq 0.98$ in DMF. A similar emission quenching has been determined for dyads with a strong proclivity for photoinduced charge separation, such as a porphyrin attached to fullerene C_{60}.[31] This observation is consistent with the HOMO−1→LUMO character computed for the transitions at 500 and 399 nm, responsible for the intramolecular charge-transfer donation from the electron-rich aromatic ring to the chlorin system.

Electrochemical properties

The redox behavior of $TPCF_{20}$-NMe_2 and the stabilities of the radical ions were studied by CV in DMF. Figure 4 shows the redox behavior of $TPCF_{20}$-NMe_2. In the regime of negative potentials, two reversible reduction waves at $E_{1/2} = -0.77$ and −1.28 V were detected. Both cathodic processes correspond to the formation of a radical anion of the chlorin ring, followed by a second one-electron reduction generating the dianion of the macrocycle.[32] Concomitantly, the redox response corresponding to the anodic process, in the regime of positive potentials, showed two oxidation processes. One of them, centered at 0.84 V, was assigned to one-electron abstraction from the *N*,*N*-dimethylaminophenyl unit, while the other process at 1.14 V could be ascribed to oxidation of the chlorin ring.[33,34] Complementary reduction peaks in the reverse sweep were not observed, indicating an i_p backward/i_p forward ratio of less than one, which evidences an irreversible oxidation process under the studied conditions. In addition, comparing the cathodic and anodic processes, the profile and height of the current peak at 1.14 V exceed expectation for a one-electron process. This peak can be assigned to oxidation of the tetrapyrrolic ring, leading to sequential radical cation and dication formation.[35] On the other hand, it is noteworthy that a value of 1.91 V could be calculated from the difference between the reduction and oxidation potentials corresponding to the tetrapyrrolic macrocycle, in reasonably good agreement with E_s (Table 3).

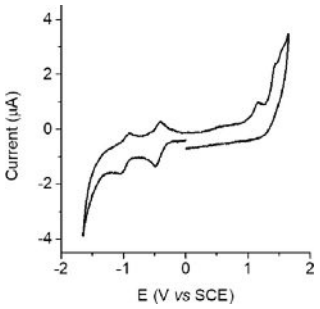

Figure 4. Cyclic voltammogram of $TPCF_{20}$-NMe_2 (1 mM) in nitrogen-purged DMF containing 0.1 M TBAHFP at a Pt working electrode; scan rate: 100 mV s^{-1}.

Therefore, the decrease in the fluorescence emission observed for $TPCF_{20}$-NMe_2 may be due to a PeT process between the electron-donating *N*,*N*-dimethylaminophenyl group and the electron-accepting macrocycle. The free-energy change for the initial charge separation giving $TPCF_{20}^{\bullet-}$-$NMe_2^{\bullet+}$ was calculated from the energies of the radical ion pair and the singlet state. For this, the simplified Rehm–Weller equation $\Delta G_{eT} = e[E_0(Am^{\bullet+}/Am) - E_0(chlorin/chlorin^{\bullet-})] - E_s$ was used, where $E_0(Am^{\bullet+}/Am)$ is the first oxidation potential of the donor (0.84 V vs. SCE), $E_0(chlorin/chlorin^{\bullet-})$ is the first reduction potential of the acceptor (−0.77 V vs. SCE), and E_s is the singlet-state energy of the chlorin (1.90 eV, Table 3).[36,37] For the initial charge transfer from $^1TPCF_{20}$-NMe_2* to the *N*,*N*-dimethylaminophenyl residue, the value of ΔG_{eT} is exergonic by about −0.29 eV. The negative value of ΔG_{eT} implies that PeT occurs as an exothermic process from the singlet excited state of $TPCF_{20}$-NMe_2. Similar values have previously been reported for PeT processes in electron donor–acceptor dyads.[31,37]

Fluorescence properties in acidified media

Taking into account that the formation of a photoinduced charge-separated state can be avoided by protonation of the amine group, fluorescence emission studies were carried out by the addition of different concentrations of HCl in DMF. As can be observed in Figure 5 A, acidification of the medium leads to a considerable increase in the fluorescence intensity

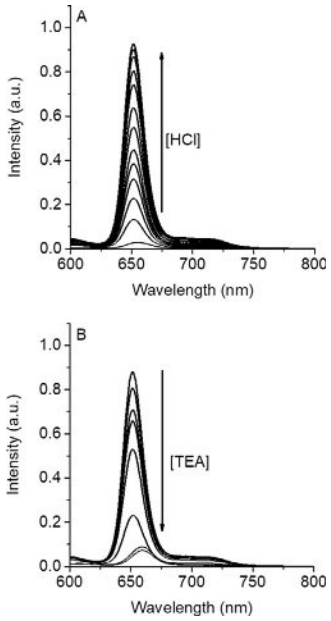

Figure 5. Fluorescence emission spectra of $TPCF_{20}$-NMe_2 in DMF in the presence of increasing concentrations of (A) HCl: 0, 0.012, 0.024, 0.036, 0.047, 0.059, 0.083, 0.118, 0.176, 0.233, 0.347, 0.458, 0.567 M and (B) TEA: 0, 0.084, 0.167, 0.247, 0.279, 0.341, 0.418, 0.508, 0.623 M (λ_{exc} = 507 nm).

of $TPCF_{20}$-NMe_2. This effect could clearly be observed in cuvettes exposed to UV light (Figure S4B). From these results, a Φ_F value of 0.15 ± 0.02 was determined for $TPCF_{20}$-NMe_2 in DMF/HCl at the maximum fluorescence intensity. Under these conditions, protonation of the amine group prevents PeT, and the fluorescence emission of $TPCF_{20}$-NMe_2 attains a similar value to that for $TPCF_{20}$ (Table 1). Conversely, the addition of triethylamine (TEA) restores the basicity of the amine group and the fluorescence emission is switched off (Figure 5 B). Under basic conditions, however, free hydroxide ions can irreversibly react at the *para* positions of the pentafluorophenyl groups of $TPCF_{20}$-NMe_2 by nucleophilic aromatic substitution.[38] A similar increase in fluorescence emission was found when the probe was dissolved in water. In this case, it was possible to monitor pH variation upon the addition of acid or base (see Figure S5 A in the Supporting Information). The macrocycle of $TPCF_{20}$-NMe_2 bears two amino groups of different basicities (*N*-methylpyrrolidine, pK_a = 10.46, and *N*,*N*-dimethylaniline, pK_a = 5.07).[39,40] Thus, initial protonation of the aliphatic amine with decreasing pH, followed by a second protonation of the aromatic amine at lower pH, is to be expected. The fluorescence is enhanced with decreasing pH and returns to the off state at near-neutral pH. The fluorescence intensity increases 30-fold in an acidic medium with respect to neutral pH. Similar behavior has previously been observed in a series of amino-BODIPY derivatives.[41] The fluorescence of these BODIPY dyes was quenched at neutral or basic pH due to PeT; however, upon protonation of the aniline nitrogen atom, the fluorescence intensity increased drastically. An acidification–neutralization–re-acidification cycle of $TPCF_{20}$-NMe_2 (see Figure S5 B) was also performed, demonstrating the reversible conversion of the molecule under these severe conditions. Evidently, at neutral pH, the *N*-methylpyrrolidine ring can remain protonated, but not the aniline derivative.

Triplet excited-state formation

Upon excitation of $TPCF_{20}$-NMe_2 with a 355 nm Nd:YAG laser operating at 12 mJ in an Ar-saturated atmosphere, no transients were detected when the experiment was performed in DMF without the addition of acid (Figure S6). However, transient absorption spectra for the acid-activated chlorin showed the appearance of two positive peaks in the regions 300–350 and 430–500 nm (Figure 6). A negative band, indicating

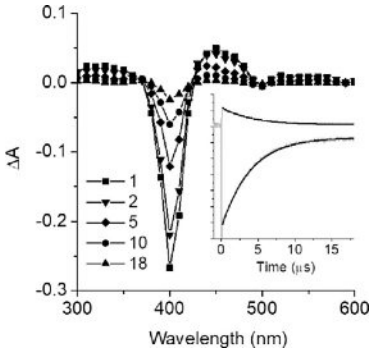

Figure 6. Transient absorption spectra of $TPCF_{20}$-NMe_2 in Ar-saturated DMF previously activated with 0.567 M HCl upon 355 nm laser excitation at 12 mJ/pulse; [$TPCF_{20}$-NMe] = 6 μM ($A^{[355]}$ = 0.24). Inset: absorption decay monitored at 450 nm and rise at 400 nm.

bleaching of the ground state, was also observed in the region 360–430 nm. This band increased as the positive bands decreased, giving rise to a distinct isosbestic point, thus indicating that only the singlet ground state (S_0) and the triplet state (T_1) are involved in the process. The triplet-state lifetime was determined as 5 μs by fitting either the decay at 400 nm or the rise at 450 nm with a single exponential (Figure 6, inset). This value is similar to those previously reported for other fluorinated chlorins.[26] Formation of a triplet excited state depending on the acidity of the medium has also been observed in dimethylaminostyryl-BODIPY–C_{60} dyads.[42] Thus, the triplet excited state was quenched by intramolecular PeT in a polar solvent. In the presence of acid, the amino group was protonated, preventing the PeT process and restoring the triplet excited state. Subsequently, the triplet–triplet absorption time profile of $TPCF_{20}$-NMe_2 at 450 nm was monitored as a function of acid concentration. At this wavelength, the difference in absorbance (ΔA) is directly related to the concentration of triplet-state species. This result is illustrated in Figure 7, which shows how triplet absorption increases with the acidity of the medium, following a sigmoidal trend.

Generation of $O_2(^1\Delta_g)$

Intrigued by the effect of acid addition on the photophysical properties of $TPCF_{20}$-NMe_2, the photosensitization of $O_2(^1\Delta_g)$ was evaluated by a direct method. Thus, $O_2(^1\Delta_g)$ phosphores-

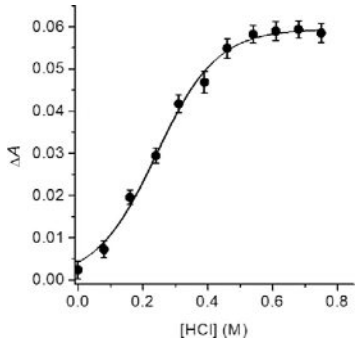

Figure 7. Maximum intensity corresponding to the transient decay of $TPCF_{20}$-NMe_2 in Ar-saturated DMF as a function of [HCl]. [$TPCF_{20}$-NMe] = 6 μM ($A^{[355]}$ = 0.24). A pulsed laser operating at 12 mJ/pulse and a wavelength of 355 nm was employed to excite the sample.

cence was monitored at 1270 nm following the incremental addition of HCl. In the presence of air, the emission signal of the $O_2(^1\Delta_g)$ formed after laser excitation of $TPCF_{20}$-NMe_2 in acidified DMF showed a first-order exponential decay. Typical results for $TPCF_{20}$-NMe_2 are shown in Figure 8A. A value of 19.4 μs was calculated for the excited-state lifetime of $O_2(^1\Delta_g)$ in this medium, in good agreement with the value obtained in pure DMF.[43,44] The initial $O_2(^1\Delta_g)$ emission intensities (I_0) were calculated from extrapolation to zero time (determined by the laser shot). Figure 8B shows the increase in $O_2(^1\Delta_g)$ phosphorescence intensity with acidification of the medium. It is important to note that, with the addition of HCl, I_0 was about 30-fold higher in the acidified medium than in pure DMF. Overall,

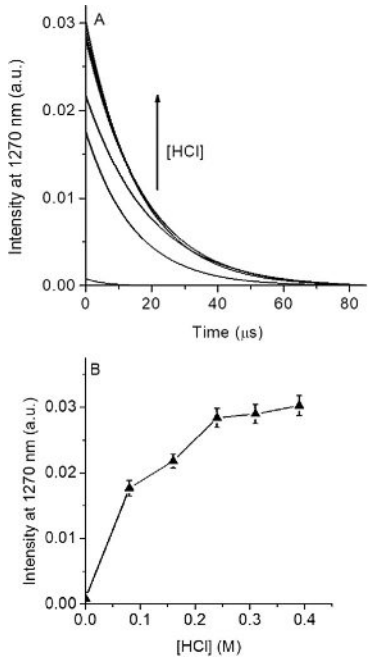

Figure 8. (A) Decay traces of $O_2(^1\Delta_g)$ emission at 1270 nm photosensitized by $TPCF_{20}$-NMe_2 in DMF at different HCl concentrations: 0, 0.080, 0.160, 0.240, 0.310, 0.390 M in air-saturated solutions and (B) initial $O_2(^1\Delta_g)$ phosphorescence emission intensities as a function of [HCl]; [$TPCF_{20}$-NMe] = 6 μM ($A^{[355]}$ = 0.24). A pulsed laser operating at 6 mJ/pulse and a wavelength of 355 nm was employed to excite the sample.

laser flash photolysis studies together with direct detection of $O_2(^1\Delta_g)$ phosphorescence evidenced the reliable response of $TPCF_{20}$-NMe_2 to the acidity of the medium. Thus, an initially deactivated photosensitizer that operates through a PeT quenching mechanism can be efficiently switched on and converted into a powerful $O_2(^1\Delta_g)$ photosensitizer after protonation of the amine group, leading to PeT deactivation.[42,45]

After acidic activation of $TPCF_{20}$-NMe_2, a reliable value for the $O_2(^1\Delta_g)$ quantum yield (Φ_Δ) was determined in DMF containing HCl (0.567 M). Previously reported $TPCF_{20}$, lacking the tertiary aniline moiety, was used as a reference to calculate the value of Φ_Δ for $TPCF_{20}$-NMe_2.[17] On a point-by-point basis, by varying the laser power and recording the phosphorescence decays at 1270 nm, it was possible to plot maximum intensity as a function of laser power (Figure 9). The ratio between the two slopes yielded a value of $\Phi_\Delta = 0.36 \pm 0.03$ in DMF/acidic medium for $TPCF_{20}$-NMe_2.

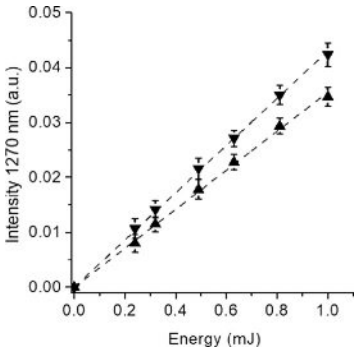

Figure 9. Intensity of $O_2(^1\Delta_g)$ phosphorescence for $TPCF_{20}$-NMe (▲) and $TPCF_{20}$ (▼) as a function of laser power in air-saturated DMF/HCl (0.567 M) solutions. [$TPCF_{20}$-NMe_2] = 6 μM ($A^{[355]}$ = 0.24). A pulsed laser operating at a wavelength of 355 nm was employed to excite the sample.

On the other hand, photo-oxidation of DMA induced by chlorins was evaluated in DMF under aerobiosis, following the decay of its band at 380 nm due to formation of the 9,10-*endo*-peroxide product (Figure 10A).[46] Considering that DMA quenches $O_2(^1\Delta_g)$ exclusively through chemical reaction, it can be used to determine the ability of chlorins to produce $O_2(^1\Delta_g)$.[47] The observed rate constants (k_{obs}) were calculated from first-order kinetic plots of DMA absorption versus time. As is evident from Table 4, $TPCF_{20}$ photosensitized the decomposition of DMA at a slower rate than that with TMPP, which was used as a reference.[46] In contrast, no photo-oxidation of DMA was detected in the presence of $TPCF_{20}$-NMe_2 under these conditions. The values of Φ_Δ were calculated by comparing the slope for $TPCF_{20}$ with that for TMPP in the plots shown in Figure 10A. The production of $O_2(^1\Delta_g)$ sensitized by $TPCF_{20}$ was very similar to that previously reported in DMF (Table 4).[17] As noted above, $TPCF_{20}$ and $TPCF_{20}$-NMe_2 show significant differences in the value of Φ_Δ. Thus, $TPCF_{20}$-NMe_2 induces almost negligible production of $O_2(^1\Delta_g)$ compared to $TPCF_{20}$ in DMF.

Moreover, photodecomposition of DMA mediated by chlorins was investigated in DMF acidified with HCl (0.567 M). From

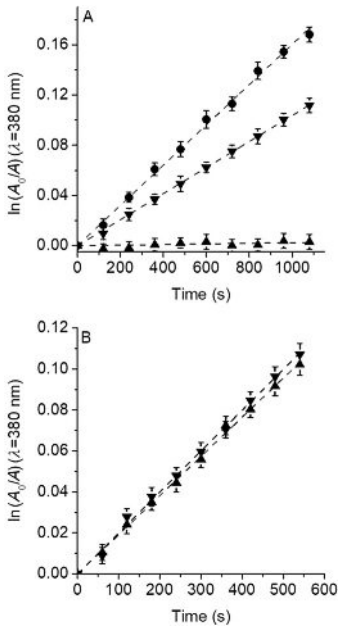

Figure 10. First-order plots for the photo-oxidation of DMA photosensitized by (A) $TPCF_{20}$-NMe_2 (▲), $TPCF_{20}$ (▼), and TMPP (●) in DMF and (B) $TPCF_{20}$-NMe_2 (▲) and $TPCF_{20}$ (▼) in DMF/HCl (0.567 M); $\lambda_{irr} = 507$ nm.

Table 4. Kinetic parameters for the photo-oxidation reaction of DMA (k_{obs}) and singlet molecular oxygen quantum yields (Φ_Δ) in DMF and acidified DMF.

Photosensitizer	k_{obs}^{DMA} (s^{-1})[a]	Φ_Δ[a]	k_{obs}^{DMA} (s^{-1})[d]
TMPP	$(1.60 \pm 0.02) \times 10^{-4}$	0.65[b]	–
$TPCF_{20}$	$(1.04 \pm 0.02) \times 10^{-4}$	0.42 ± 0.02[c]	$(2.00 \pm 0.06) \times 10^{-4}$
$TPCF_{20}$-NMe_2	–	–	$(1.91 \pm 0.05) \times 10^{-4}$

[a] In DMF; [b] from ref. [46]; [c] $\Phi_\Delta = 0.41$ from ref. [17]; [d] in DMF/HCl (0.567 M).

the plots in Figure 10B, values of k_{obs}^{DMA} were calculated for DMA decomposition in this medium. As can be observed in Table 4, the decomposition of DMA sensitized by these chlorins followed the tendency found by direct $O_2(^1\Delta_g)$ measurements. $TPCF_{20}$-NMe_2 is an efficient photosensitizer for generating $O_2(^1\Delta_g)$ in this acidified DMF medium. With protonation of the amino group, PeT was inhibited, increasing the intersystem crossing and hence the production of $O_2(^1\Delta_g)$. Moreover, the photo-oxidation of DMA mediated by $TPCF_{20}$-NMe_2 showed a similar reaction rate to that obtained with $TPCF_{20}$, indicating that PeT was negligible in this acidified medium.

Fluorescence images and photosensitized inactivation of *E. coli*

The pH-dependent switching capacity of $TPCF_{20}$-NMe_2 as a fluorescent probe and photosensitizer was evaluated in relation to *E. coli* inactivation. First, images of cells treated with 10 μM $TPCF_{20}$-NMe_2 were obtained by fluorescence microscopy at pH 7.2 and pH 2. For *E. coli* cells at pH 7.2, no fluorescence emission was detected. However, fluorescence emission of $TPCF_{20}$-NMe_2 bound to the *E. coli* cells was observed at pH 2. Figure 11 shows typical bright-field (A) and fluorescence (B) microscope images of *E. coli* at pH 2. The characteristic red emission was seen from the cells, as previously observed in different microorganisms.[48,49] Thus, this emission can be assigned to $TPCF_{20}$-NMe_2 bound to *E. coli* cells, which remains off at neutral pH and is turned on at acidic pH.

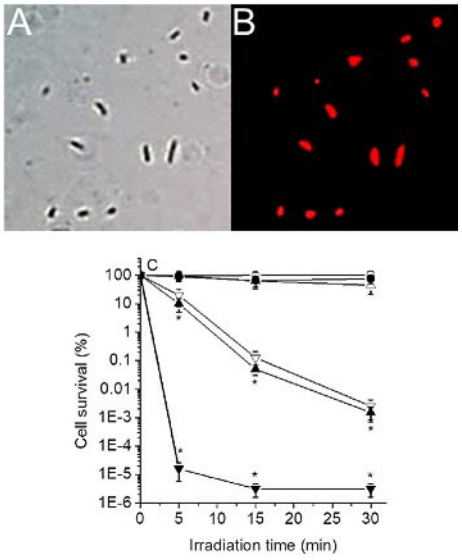

Figure 11. Microscope images of *E. coli* incubated with 10 μM $TPCF_{20}$-NMe_2 for 10 min at 37 °C in the dark at pH 2: (A) cells under bright field and (B) fluorescence emission (100× microscope objective). (C) Survival of *E. coli* (ca. 10^8 CFU mL^{-1}) treated with 10 μM $TPCF_{20}$-NMe_2 at different pH values 7.2 (●), 3.0 (▲), and 2.0 (▼) and irradiated with visible light for 5, 15, and 30 min (*$p < 0.05$, compared with control). Irradiated control culture without photosensitizer at the same pH values 7.2 (○), 3.0 (△), and 2.0 (▽).

Next, photosensitized inactivation of *E. coli* mediated by $TPCF_{20}$-NMe_2 was investigated after different irradiation periods with visible light at different pH values. Survival curves are shown in Figure 11C. No toxicity was observed for *E. coli* cells treated with 10 μM $TPCF_{20}$-NMe_2 for 30 min in the dark (results not shown). Moreover, the viability of the microbial cells was not affected by irradiation without the photosensitizer at pH 7.2 or 3.0 (Figure 11C). At pH 2, a reduction of 3 log units was found after incubation for 30 min for cells treated with $TPCF_{20}$-NMe_2 in the dark or irradiated without the addition of chlorin, indicating some toxicity of this acidic medium. On the other hand, photoinactivation of *E. coli* by $TPCF_{20}$-NMe_2 was negligible at pH 7.2. The differences between all tested combinations were not statistically significant ($p > 0.05$) after 5, 15, and 30 min of irradiation. In contrast, cell survival was dependent on irradiation times in an acidified medium. For all irradiation times, survival was significantly reduced compared to the control ($p < 0.05$). A reduction of 3 log units in the *E. coli* survival was determined at pH 3 after 15 min of irradiation, and a 4.5 log unit (99.997%) decrease was observed after an irradiation time of 30 min. After a short irradiation time of 5 min, $TPCF_{20}$-NMe_2 induced a 6 log unit decrease in cell survival at

pH 2.0. This chlorin achieved practically complete eradication after 15 min of irradiation. These values mean a bacterial inactivation greater than 99.9999%. Under similar conditions, the photocytotoxic effect elicited by $TPCF_{20}$-NMe_2 at pH 2.0 was higher than that previously found using 5 μM 5,10,15,20-tetrakis[4-(3-*N*,*N*-dimethylaminopropoxy)phenyl]porphyrin or its chlorin analogue after short irradiation periods.[18] Moreover, the photokilling activity of $TPCF_{20}$-NMe_2 at pH 3.0 was considerably higher than that found for *E. coli* cells treated with 5 μM 5,10-di(4-methylphenyl)-15,20-di(4-*N*,*N*,*N*-trimethylammoniumphenyl)porphyrin.[50] The PDI activity of $TPCF_{20}$-NMe_2 at pH 2.0 was also similar to that obtained with 5 μM 5,10,15,20-tetrakis(4-*N*,*N*,*N*-trimethylammoniumphenyl)porphyrin, which represents a recognized photosensitizer for eradicating microorganisms by PDI.[50] Moreover, it has previously been demonstrated that $TPCF_{20}$ immobilized on solid supports displays an improved efficiency for photoinactivation of *E. coli*.[51] However, it should be noted that most PDI studies have been conducted at physiological pH, and to the best of our knowledge there have been no studies concerning actual applications of chlorins as antimicrobial photosensitizers in acid media.[6,9] This can be explained by taking into account that most tetrapyrrolic macrocycles do not have suitable characteristics for use in PDI at low pH, since their inner N atoms can be protonated, leading to loss of the appropriate spectroscopic and photodynamic features. $TPCF_{20}$-NMe_2 remains inactive at neutral pH and the photoinactivation capacity can be efficiently switched on in acidic media to eradicate bacteria.

Conclusion

The new $TPCF_{20}$-NMe_2 comprises a chlorin macrocycle incorporating a *syn* adduct of a pyrrolidine-fused ring bearing a C-linked *N*,*N*-dimethylaminophenyl residue. In this structure, the macrocycle is substituted by four pentafluorophenyl electron-withdrawing groups at the *meso* positions and by an electron-donating amine group. Therefore, PeT takes place from the amine segment to the chlorin macrocycle, and this process effectively competes with fluorescence emission and intersystem crossing, preventing formation of the triplet excited state. However, acidification of the medium leads to protonation of the amino group, which in turn leads to an enhancement of the radiative processes. Large increases in the fluorescence emission and $O_2(^1\Delta_g)$ production were elicited upon the addition of acid. Protonation of the amine group avoids quenching of the singlet and triplet states and restores the ability of the compound to photosensitize singlet molecular oxygen, $O_2(^1\Delta_g)$.

A large number of microorganisms, including *E. coli*, can survive under extreme acid conditions. However, most of the photosensitizers proposed for PDI have been investigated under conditions close to physiological pH. In acidic media, $TPCF_{20}$-NMe_2 proved to be highly efficient in eradicating *E. coli*, even within short irradiation times. The main advantage of $TPCF_{20}$-NMe_2 is that it can remain inactive at neutral pH, avoiding photocytotoxic damage, but becomes an effective fluorophore and photosensitizer at acid pH. Although acid pH values are very harsh conditions, some microorganisms can still overcome them, even in human gastric juice. Strains of *E. coli* resistant to acid media and antibiotics can be dangerous to human health, inducing diseases in the highly acidic mammalian stomach. In this context, PDI of microorganisms using photosensitizers that are only active in acid media can be proposed as an alternative therapy to inactivate these microorganisms. Therefore, $TPCF_{20}$-NMe_2 represents an interesting molecular structure because protonation of the amino group can be used as an off/on molecular switch, activating red fluorescence emission and photodynamic activity to inactivate microbial cells.

Experimental Section

General

Proton nuclear magnetic resonance spectra were acquired on a Bruker Avance 300 FT-NMR spectrometer. Mass spectra were measured on a Bruker micrO-TOF-QII spectrometer (Bruker Daltonics, MA, USA) equipped with an ESI source (ESI-MS). Absorption spectra were recorded on a Shimadzu UV-2401 PC spectrometer (Shimadzu Corporation, Tokyo, Japan). Fluorescence spectra were measured on a Spex FluoroMax spectrofluorimeter (Horiba–Jobin-Yvon Inc., Edison, NJ, USA). Fluence rates were measured using a Laser Mate-Q radiometer (Coherent, Santa Clara, CA, USA). Photolyses of substrates were investigated with a Cole–Parmer illuminator 41720-series containing a 150 W halogen lamp (Cole–Parmer, Vernon Hills, IL, USA), light from which was passed through a high-intensity grating monochromator (Photon Technology Instrument, Birmingham, NJ, USA) with a fluence rate of 0.82 mW cm^{-2} at 507 nm. *E. coli* cells were irradiated with a Novamat 130 AF incorporating a 150 W halogen lamp (Braun Photo Technik, Nürnberg, Germany). The wavelength range 350–800 nm was selected by optical filters with a fluence rate of 90 mW cm^{-2}. Chemicals from Sigma–Aldrich (Milwaukee, WI, USA) were used without further purification. TMPP and $TPPF_{20}$ were also purchased from Sigma–Aldrich. Silica gel thin-layer chromatography (TLC) plates (250 μm) were acquired from Analtech (Newark, DE, USA). Silica gel 60 (0.040–0.063 mm, 230–400 mesh) from Merck (Darmstadt, Germany) was used for flash column chromatography.

Synthesis of chlorin derivatives

N-Methylglycine (40 mg, 0.45 mmol) and 4-(dimethylamino)benzaldehyde (104 mg, 0.69 mmol) were added to a stirred solution of $TPPF_{20}$ (80 mg, 0.082 mmol) in anhydrous toluene (20 mL) and the reaction mixture was heated under reflux for 18 h under an argon atmosphere. The solution was then cooled to room temperature and the solvent was evaporated under reduced pressure. The resulting solid residue was purified by flash column chromatography (silica gel; toluene → toluene/ethyl acetate, 4:1) to afford 24 mg (28%) of pure $TPCF_{20}$ and 30 mg (32%) of pure $TPCF_{20}$-NMe_2 as the first and second eluted green bands, respectively. $TPCF_{20}$: dark-green solid, TLC (silica gel; toluene/ethyl acetate, 9:1): $R_f = 0.41$; ^{1}H NMR ($CDCl_3$, TMS) (Figure S7): $\delta = -1.80$ (s, 2H; NH), 2.18 (s, 3H; N-CH_3), 2.50–2.58 (m, 2H; pyrrolidine-H), 3.14 (t, 2H, $J = 8.0$ Hz; pyrrolidine-H), 5.25 (t, 2H, $J = 4.9$ Hz; β-H; reduced pyrrole), 8.39 (d, 2H, $J = 5.0$ Hz; β-H), 8.48 (s, 2H; β-H), 8.71 ppm (d, 2H, $J = 5.0$ Hz; β-H); ESI-MS: *m*/*z*: 1032.1240 $[M+H]^+$, 1054.1060 $[M+Na]^+$ (calcd for $C_{47}H_{17}F_{20}N_5$: 1031.1165). $TPCF_{20}$-NMe_2: dark-green solid, TLC (silica gel; toluene/ethyl acetate, 9:1) analysis: $R_f = 0.26$; ^{1}H NMR ($CDCl_3$, TMS): $\delta = -1.62$ (s, 1H; NH), -1.51 (s, 1H; NH), 1.75 (s, 3H; N-CH_3), 2.56 (s, 6H; N-$(CH_3)_2$), 2.87 (dd, 1H, $J = 7.3$ and 9.7 Hz; pyr-

rolidine-H), 3.56 (d, 1H, $J=9.7$ Hz; pyrrolidine-H), 3.63 (d, 1H, $J=8.8$ Hz; pyrrolidine-H), 5.36 (dd, 1H, $J=7.3$ and 8.2 Hz, β-H; reduced pyrrole), 5.65 (d, 2H, $J=8.8$ Hz; benzene ring), 5.68 (dd, 1H, $J=8.2$ and 8.8 Hz, β-H; reduced pyrrole), 5.85 (d, 2H, $J=8.8$ Hz; benzene ring), 8.12 (d, 2H, $J=5.0$ Hz; β-H), 8.41 (d, 2H, $J=4.7$ Hz; β-H), 8.45 (AB, 2H; β-H), 8.51 (d, 2H, $J=5.0$ Hz; β-H), 8.69 ppm (d, 2H, $J=4.7$ Hz; β-H); ESI-MS: *m/z*: 1151.1976 $[M+H]^+$, 1173.1790 $[M+Na]^+$ (calcd for $C_{55}H_{26}F_{20}N_6$: 1150.1900).

Theoretical calculations

All DFT calculations were performed with the Gaussian 09 suite of programs (Gaussian, Wallingford, CT) with the B3LYP functional coupled with the 6-31G* basis set. Geometries for all structures were fully optimized, and frequency calculations were used to confirm the nature of the stationary points. In all cases, positive definite Hessian matrices were found. The reported thermochemical properties include zero-point energies (ZPEs) without scaling, calculated at 1 atm and 298.15 K. Exhaustive conformational searches were performed to locate the minimum-energy conformers of all of the structures. Initially, a large number of geometries were generated using the conformational search modules of Hyperchem (Spartan'08, Wavefunction, Irvine, CA) and Spartan'14 (Hyperchem Professional Release 7.52, Hypercube, Gainesville, FL) with the MM+ and MMFF force fields, respectively. All structures were then successively re-optimized at the RHF/3–21G and B3LYP/6–31G* levels of theory. NMR spectra were calculated by the *gauge-including atomic orbitals* (GIAO) method,[52–55] which was chosen to solve the gauge origin problem.[56,57] Magnetic shielding constants (σ) were computed at the mPW1PW91/6–31+G** level of theory, using the polarizable continuum model (PCM) with chloroform as solvent to include the solvent effect.[58] Chemical shifts (δ) were computed using the multi-standard approach (MSTD), using methanol and benzene as reference standards for protons attached to sp^3 and sp^2 hybridized carbon atoms, respectively.[59,60] DP4+ calculations were carried out using the Excel toolbox available free of charge at sarotti-NMR.weebly.com, or as part of the supporting information of the original paper.[61] FMO and TDDFT calculations were carried out at the CAM-B3LYP/6-31G* level of theory. This hybrid exchange-correlation functional is the long-range corrected version of B3LYP that accounts for the true asymptotic behavior at long interelectronic distances.[62]

Spectroscopic studies

UV/Vis absorption and fluorescence spectra of the photosensitizers were recorded from solutions in quartz cell of path length 1 cm at 25.0±0.5 °C. Fluorescence emission spectra were obtained by exciting the samples at $\lambda_{exc}=507$ nm. The energy of the singlet state (E_s) was determined from the intersection of the normalized absorption and fluorescence spectra. The fluorescence quantum yield (Φ_F) of each chlorin was calculated by comparison of the area below the corrected emission spectrum with that below the spectrum of TMPP as a reference ($\Phi_F=0.14$) in *N*,*N*-dimethylformamide (DMF).[46] The absorbances of the chlorins and the reference (<0.05) were matched at the excitation wavelength and the areas under the emission spectra were integrated in the range 600–800 nm.

Electrochemical measurements

Cyclic voltammetry (CV) experiments were performed with an Autolab potentiostat–galvanostat (Electrochemical Instruments, Utrecht, The Netherlands) using a Pt working electrode, a silver wire reference electrode, and a Pt coil counter electrode.[63] Electrochemical studies of $TPCF_{20}$-NMe_2 were carried out at room temperature by CV in deoxygenated DMF containing 0.1 M tetra-*n*-butylammonium hexafluorophosphate (TBAHFP) as the supporting electrolyte. Ferrocene was used as an internal standard in all of the voltammetric experiments. The potential axis was calibrated against the formal potential for the saturated calomel electrode (SCE). Solutions were deoxygenated by argon bubbling, and all measurements were conducted at a scan rate of 100 mV s^{-1}.

Laser flash photolysis studies

Transient absorption measurements on $TPCF_{20}$-NMe_2 were performed in argon-saturated DMF solution containing different concentrations of HCl (0–0.567 M) by laser flash photolysis. A Spectron SL400 Nd:YAG laser generating 355 nm laser pulses (12 mJ per pulse, ca. 18 ns FWHM) was the excitation source. The experiments were conducted using rectangular quartz cells with right-angle geometry. The concentration was kept low to avoid triplet–triplet annihilation. The laser beam was defocused to cover all of the path length (10 mm) of the analyzing beam from a 150 W Xe lamp. A PTI monochromator coupled to a Hamamatsu R666 PM tube was used as the detection system. The signals were acquired and averaged by a digital oscilloscope (Hewlett–Packard 54504) and then transferred to a computer. All determinations were performed at 25 °C, and the solutions were deoxygenated by bubbling with solvent-saturated high-purity argon for at least 20 min.

Generation of $O_2(^1\Delta_g)$

Photosensitization of $O_2(^1\Delta_g)$ was assessed by measuring its phosphorescence decay signal by means of a time-resolved detection method (TRPD). The excitation source was the aforementioned Nd:YAG laser operating at 355 nm, and the laser power was 6 mJ/pulse. The emitted radiation (mainly 1270 nm) was detected at right angles with a Judson J16/8Sp amplified germanium detector, after passage through appropriate filters. The output of the detector was coupled to a digital oscilloscope (Hewlett–Packard HP-54504A). About ten shots were usually needed for averaging decay times, in order to get a good signal-to-noise ratio. No changes in the absorption spectra of the samples were observed after these experiments, thus indicating no significant photodegradation of the photosensitizer. The averaged signals were analyzed as single-exponential decays. The absorbance of the sample and reference were matched at the irradiation wavelength. Measurements of these solutions under the same conditions afforded Φ_Δ for the studied chlorins by direct comparison of the slopes, in the linear region, of plots of the phosphorescence amplitude extrapolated to zero time against the total laser energy. $TPPF_{20}$ was used as a reference ($\Phi_\Delta=0.41$ in DMF).[17]

Steady-state photolysis

Solutions of 9,10-dimethylanthracene (DMA, 35 μM) and photosensitizer in DMF (2 mL) were irradiated in 1 cm path length quartz cells using monochromated light at $\lambda_{irr}=515$ nm, with a photosensitizer absorption of 0.1 at the irradiation wavelength. The kinetics of DMA photodecomposition was analyzed by following the decrease in absorbance (A) at $\lambda_{max}=380$ nm. Values of k_{obs}^{DMA} were determined by a linear least-squares fit of a semi-logarithmic plot of $\ln A_0/A$ vs. time. Quantum yields of $O_2(^1\Delta_g)$ production (Φ_Δ) were calculated by comparing k_{obs} for the corresponding chlorin with that for TMPP, which was used as a reference ($\Phi_\Delta=0.65$).[46] Measurements of the sample and reference under the same conditions

afforded Φ_Δ for the photosensitizer by direct comparison of the slopes in the linear regions of the plots. Photo-oxidation of DMA in DMF/HCl (0.567 M) was performed as described for the experiments in DMF.

E. coli culture conditions

The strain of *E. coli* used (EC7) was previously characterized and identified.[18] Bacterial cells were aerobically cultured overnight under sterile conditions at 37 °C in tryptic soy (Britania, Buenos Aires, Argentina) broth (4 mL). An aliquot (40 μL) of the bacterial culture was aseptically transferred to fresh tryptic soy broth (4 mL) and the mixture was incubated at 37 °C to induce the exponential phase of growth (absorbance 0.6 at 660 nm). Cultures were centrifuged (3000 rpm for 15 min), and then the cells were re-suspended in 10 mM phosphate-buffered saline (PBS, pH 7.2; 4 mL), corresponding to about 10^8 colony-forming units (CFU) mL^{-1}. This procedure was repeated three times to remove components from the broth.

Photosensitized inactivation of *E. coli* and fluorescence images

Cell suspensions of *E. coli* (2 mL, ca. 10^8 CFU mL^{-1}) in PBS (Pyrex culture tubes, 13×100 mm) were centrifuged (3000 rpm for 10 min). The cell pellets were re-suspended in PBS (2 mL). Acidified cells were obtained by re-suspending the pellets in aqueous solution at pH 3.0 or pH 2.0 for 10 min at 37 °C. The acid media were prepared by the addition of HCl from a stock solution 0.5 mM HCl. Cells were treated with 10 μM $TPCF_{20}$-NMe_2 for 10 min in the dark at 37 °C. $TPCF_{20}$-NMe_2 was added from a 1.2 mM stock solution in DMF. Thereafter, 200 μL of each cell suspension was transferred to a 96-well microtiter plate (Deltalab, Barcelona, Spain). Cell suspensions were immediately irradiated with visible light for different times. After irradiation, the *E. coli* cells were serially diluted 10-fold with PBS. Cell suspensions were quantified in triplicate by the spread plate method. Viable bacteria were examined and the number of CFU was counted on a tryptic soy agar plate after incubation for about 24 h at 37 °C in the dark. For fluorescence microscopy experiments, bacteria were grown and treated under the same conditions as used for PDI assays. Microscopic observations were made with a Zeiss Axiostar Plus fluorescence microscope (Carl Zeiss, Oberkochen, Germany). Images were acquired in bright-field and fluorescence modes using a Filter Set 05 (Carl Zeiss).

Statistical analysis

Control experiments with *E. coli* cells were carried out in the presence and absence of $TPCF_{20}$-NMe_2 in the dark and by irradiating cells in the absence of photosensitizer. The amount of DMF (< 1% v/v) used in each experiment was not toxic to bacterial cells. Three values were obtained for each condition, and each experiment was separately repeated in triplicate. An unpaired *t*-test was used to establish the significance of differences between groups. Differences between means were tested for significance by one-way ANOVA. Results were considered as statistically significant with a confidence level of 95% ($p < 0.05$). Data are represented as the mean ± standard deviation of each group.

Acknowledgements

The authors are grateful to the Consejo Nacional de Investigaciones Científicas y Técnicas (CONICET, PIP-2015 1122015 0100197 CO) of Argentina, the Universidad Nacional de Río Cuarto (UNRC-SECYT PPI-2016 18/C460), and the Agencia Nacional de Promoción Científica y Tecnológica (ANPCYT, PICT 0667/16) of Argentina for financial support. D.A.H., A.M.D., A.M.S., N.S.G., S.G.B., M.E.M., and E.N.D. are Scientific Members of CONICET. D.D.F. thanks CONICET for research fellowships.

Conflict of interest

The authors declare no conflict of interest.

Keywords: chlorins · fluorescent probes · electron transfer · photosensitizers · porphyrinoids

[1] J. S. Lindsey, *Chem. Rev.* **2015**, *115*, 6534 – 6620.
[2] M. Taniguchi, J. S. Lindsey, *Chem. Rev.* **2017**, *117*, 344 – 535.
[3] J. S. Lindsey, *Acc. Chem. Res.* **2010**, *43*, 300 – 311.
[4] A. M. G. Silva, A. C. Tomé, M. G. P. M. S. Neves, A. M. S. Silva, J. A. S. Cavaleiro, *Chem. Commun.* **1999**, 1767 – 1768.
[5] G. Jiménez-Osés, J. I. García, A. M. G. Silva, A. R. N. Santos, A. C. Tomé, M. G. P. M. S. Neves, J. A. S. Cavaleiro, *Tetrahedron* **2008**, *64*, 7937 – 7943.
[6] H. Abrahamse, M. R. Hamblin, *Biochem. J.* **2016**, *473*, 347 – 364.
[7] M. Ethirajan, Y. Chen, P. Joshi, R. K. Pandey, *Chem. Soc. Rev.* **2011**, *40*, 340 – 362.
[8] M. O. Senge, *Photodiagn. Photodyn. Ther.* **2012**, *9*, 170 – 179.
[9] A. Martinez De Pinillos Bayona, P. Mroz, C. Thunshelle, M. R. Hamblin, *Chem. Biol. Drug Des.* **2017**, *89*, 192 – 206.
[10] E. Alves, M. A. Faustino, M. G. Neves, A. Cunha, J. Tome, A. Almeida, *Future Med. Chem.* **2014**, *6*, 141 – 164.
[11] T. G. St. Denis, T. Dai, L. Izikson, C. Astrakas, R. R. Anderson, M. R. Hamblin, G. P. Tegos, *Virulence* **2011**, *2*, 509 – 520.
[12] X.-Z. Li, P. Plésiat, H. Nikaido, *Clin. Microbiol. Rev.* **2015**, *28*, 337 – 418.
[13] A. C. Rios, C. G. Moutinho, F. C. Pinto, F. S. Del Fiol, A. Jozala, M. V. Chaud, M. M. D. C. Vila, J. A. Teixeira, V. M. Balcão, *Microbiol. Res.* **2016**, *191*, 51 – 80.
[14] T. P. Zabawa, M. J. Pucci, T. R. Parr, Jr., T. Lister, *Curr. Opin. Microbiol.* **2016**, *33*, 7 – 12.
[15] N. S. Soukos, M. R. Hamblin, T. Hasan, *Photochem. Photobiol.* **1997**, *65*, 723 – 729.
[16] D. C. S. Costa, M. C. Gomes, M. A. F. Faustino, M. G. P. M. S. Neves, Â. Cunha, J. A. S. Cavaleiro, A. Almeida, J. P. C. Tomé, *Photochem. Photobiol. Sci.* **2012**, *11*, 1905 – 1913.
[17] M. Q. Mesquita, J. C. J. M. D. S. Menezes, M. G. P. M. S. Neves, A. C. Tomé, J. A. S. Cavaleiro, Â. Cunha, A. Almeida, S. Hackbarth, B. Röder, M. A. F. Faustino, *Bioorg. Med. Chem. Lett.* **2014**, *24*, 808 – 812.
[18] D. D. Ferreyra, E. Reynoso, P. Cordero, M. B. Spesia, M. G. Alvarez, M. E. Milanesio, E. N. Durantini, *J. Photochem. Photobiol. B* **2016**, *158*, 243 – 251.
[19] U. Kanjee, W. A. Houry, *Annu. Rev. Microbiol.* **2013**, *67*, 65 – 81.
[20] J. R. Huddleston, *Infect. Drug Resist.* **2014**, *2014*, 167 – 176.
[21] D. Hwang, S. M. Kim, H. J. Kim, *Int. J. Antimicrob. Agents* **2017**, *49*, 81 – 87.
[22] F. S. Vinhado, M. E. F. Gandini, Y. Iamamoto, A. M. G. Silva, M. M. Q. Simões, M. G. P. M. S. Neves, A. C. Tomé, S. L. H. Rebelo, A. M. V. M. Pereira, J. A. S. Cavaleiro, *J. Mol. Catal. A* **2005**, *239*, 138 – 143.
[23] N. M. M. Moura, F. Giuntini, M. A. F. Faustino, M. G. P. M. S. Neves, A. C. Tomé, A. M. S. Silva, E. M. Rakib, A. Hannioui, S. Abouricha, B. Röder, J. A. S. Cavaleiro, *ARKIVOC* **2010**, *5*, 24 – 33.
[24] T. Hofmann, P. Münch, P. Schieberle, *J. Agric. Food Chem.* **2000**, *48*, 434 – 440.

[25] A. M. G. Silva, A. C. Tomé, M. G. P. M. S. Neves, J. A. S. Cavaleiro, D. Perrone, A. Dondoni, *Synlett* **2005**, *5*, 857 – 859.
[26] M. Pineiro, M. M. Pereira, A. M. d'A. Rocha Gonsalves, L. G. Arnaut, S. J. Formosinho, *J. Photochem. Photobiol. A* **2001**, *138*, 147 – 157.
[27] H. M. Rhoda, J. Akhigbe, J. Ogikubo, J. R. Sabin, C. J. Ziegler, C. Brückner, V. N. Nemykin, *J. Phys. Chem. A* **2016**, *120*, 5805 – 5815.
[28] S. S. Yamijala, G. Periyasamy, S. K. Pati, *J. Phys. Chem. A* **2011**, *115*, 12298 – 12306.
[29] L. Petit, A. Quartarolo, C. Adamo, N. Russo, *J. Phys. Chem. B* **2006**, *110*, 2398 – 2404.
[30] D. D. Ferreyra, M. B. Spesia, M. E. Milanesio, E. N. Durantini, *J. Photochem. Photobiol. A* **2014**, *282*, 16 – 24.
[31] M. B. Ballatore, M. B. Spesia, M. E. Milanesio, E. N. Durantini, *Eur. J. Med. Chem.* **2014**, *83*, 685 – 694.
[32] S. Cosnier, C. Gondran, K. Gorgy, R. Wessel, F.-P. Montforts, M. Wedel, *Electrochem. Commun.* **2002**, *4*, 426 – 430.
[33] H. Yang, D. O. Wipf, A. J. Bard, *J. Electroanal. Chem.* **1992**, *331*, 913 – 924.
[34] M. Kollmannsberger, T. Gareis, S. Heinl, J. Breu, J. Daub, *Angew. Chem. Int. Ed. Engl.* **1997**, *36*, 1333 – 1335; *Angew. Chem.* **1997**, *109*, 1391 – 1393.
[35] C.-W. Lee, H.-P. Lu, C.-M. Lan, Y.-L. Huang, Y.-R. Liang, W.-N. Yen, Y.-C. Liu, Y.-S. Lin, E. W.-G. Diau, C.-Y. Yeh, *Chem. Eur. J.* **2009**, *15*, 1403 – 1412.
[36] P. K. Poddutoori, A. S. D. Sandanayaka, N. Zarrabi, T. Hasobe, O. Ito, A. van der Est, *J. Phys. Chem. A* **2011**, *115*, 709 – 717.
[37] S. K. Das, B. Song, A. Mahler, V. N. Nesterov, A. K. Wilson, O. Ito, F. D'Souza, *J. Phys. Chem. C* **2014**, *118*, 3994 – 4006.
[38] H. R. A. Golf, H.-U. Reissig, A. Wiehe, *Eur. J. Org. Chem.* **2015**, 1548 – 1568.
[39] H. K. Hall, Jr., *J. Am. Chem. Soc.* **1957**, *79*, 5441 – 5444.
[40] M. M. Fickling, A. Fischer, B. R. Mann, J. Packer, J. Vaughan, *J. Am. Chem. Soc.* **1959**, *81*, 4226 – 4230.
[41] S. Hoogendoorn, A. E. M. Blom, L. I. Willems, G. A. van der Marel, H. S. Overkleeft, *Org. Lett.* **2011**, *13*, 5656 – 5659.
[42] L. Huang, J. Zhao, *J. Mater. Chem. C* **2015**, *3*, 538 – 550.
[43] B. Aveline, O. Delgado, D. Brault, *J. Chem. Soc. Faraday Trans.* **1992**, *88*, 1971 – 1976.
[44] S. Oelckers, T. Hanke, B. Röder, *J. Photochem. Photobiol. A* **2000**, *132*, 29 – 32.
[45] S. O. McDonnell, M. J. Hall, L. T. Allen, A. Byrne, W. M. Gallagher, D. F. O'Shea, *J. Am. Chem. Soc.* **2005**, *127*, 16360 – 16361.
[46] M. E. Milanesio, M. G. Alvarez, E. I. Yslas, C. D. Borsarelli, J. J. Silber, V. Rivarola, E. N. Durantini, *Photochem. Photobiol.* **2001**, *74*, 14 – 21.
[47] A. Gomes, E. Fernandes, J. L. F. C. Lima, *J. Biochem. Biophys. Methods* **2005**, *65*, 45 – 80.
[48] R. Dosselli, M. Gobbo, E. Bolognini, S. Campestrini, E. Reddi, *ACS Med. Chem. Lett.* **2010**, *1*, 35 – 38.
[49] H.-R. Jia, Y.-X. Zhu, Z. Chen, F.-G. Wu, *ACS Appl. Mater. Interfaces* **2017**, *9*, 15943 – 15951.
[50] N. S. Gsponer, M. B. Spesia, E. N. Durantini, *Photodiagn. Photodyn. Ther.* **2015**, *12*, 67 – 75.
[51] M. Q. Mesquita, J. C. J. M. D. S. Menezes, S. M. G. Pires, M. G. P. M. S. Neves, M. M. Q. Simões, A. C. Tomé, J. A. S. Cavaleiro, Â. Cunha, A. L. Daniel-da-Silva, A. Almeida, M. A. F. Faustino, *Dyes Pigm.* **2014**, *110*, 123 – 133.
[52] R. Ditchfield, *J. Chem. Phys.* **1972**, *56*, 5688 – 5691.
[53] R. Ditchfield, *Mol. Phys.* **1974**, *27*, 789 – 807.
[54] C. McMichael Rohlfing, L. C. Allen, R. Ditchfield, *Chem. Phys.* **1984**, *87*, 9 – 15.
[55] K. Wolinski, J. F. Hinton, P. Pulay, *J. Am. Chem. Soc.* **1990**, *112*, 8251 – 8260.
[56] N. Grimblat, A. M. Sarotti, *Chem. Eur. J.* **2016**, *22*, 12246 – 12261.
[57] M. W. Lodewyk, M. R. Siebert, D. J. Tantillo, *Chem. Rev.* **2012**, *112*, 1839 – 1862.
[58] J. Tomasi, B. Mennucci, R. Cammi, *Chem. Rev.* **2005**, *105*, 2999 – 3094.
[59] A. M. Sarotti, S. C. Pellegrinet, *J. Org. Chem.* **2009**, *74*, 7254 – 7260.
[60] A. M. Sarotti, S. C. Pellegrinet, *J. Org. Chem.* **2012**, *77*, 6059 – 6065.
[61] N. Grimblat, M. M. Zanardi, A. M. Sarotti, *J. Org. Chem.* **2015**, *80*, 12526 – 12534.
[62] T. Yanai, D. P. Tew, N. C. Handy, *Chem. Phys. Lett.* **2004**, *393*, 51 – 57.
[63] J. Durantini, M. B. Suarez, M. Santo, E. Durantini, T. Dittrich, L. Otero, M. Gervaldo, *J. Phys. Chem. C* **2015**, *119*, 4044 – 4051.

Manuscript received: January 5, 2018
Accepted manuscript online: February 5, 2018
Version of record online: March 22, 2018